COMSOL Multiphysics® Simulation of Flow in a Radial Flow Fixed Bed Reactor (RFBR)

Anthony G. Dixon*,[1], Dominic Polcari[1], Anthony Stolo[1] and Mai Tomida[1]
[1]Department of Chemical Engineering, Worcester Polytechnic Institute
*Corresponding author: 100 Institute Road, Worcester, MA 01609, agdixon@wpi.edu

Abstract: In the design of radial flow fixed bed reactors, it is important to ensure proper flow distribution through the catalyst bed. Utilizing COMSOL Multiphysics®, a 2D axisymmetric model of a conceptual radial-flow reactor design was developed and was used to evaluate flow maldistribution through the catalyst bed and the pressure drop through the reactor for the specified flow rate. Effects of different catalysts, screen sizes and flow direction were simulated. Factors which improved misdistribution, such as smaller catalyst particles, lower screen open fraction, and normal flow direction, also resulted in higher pressure drop through the reactor. The simulations indicated that design of the reactor to reduce pressure drop in the inlet and outlet channels is a major concern, while the catalyst bed specification is a trade-off between desired low pressure drop and better catalyst utilization with low maldistribution.

Keywords: Reaction engineering, radial-flow, packed bed, maldistribution, catalyst particle, velocity profiles.

1. Introduction

Radial flow packed bed reactors are used to carry out large scale catalytic chemical reactions in the petroleum and chemical industries [1]. This specific type of reactor has strong advantages for catalytic processes such as ammonia synthesis, catalytic reforming, and dehydrogenation of ethyl benzene. The ability to operate at a lower pressure drop compared to an axial flow reactor for the same volumetric flow creates opportunities for saving cost. Inside the radial flow reactor, a given gas volume enters axially then flows radially through a catalyst bed and is collected and exits axially. It is recommended to have a uniformly distributed flow over the length of the bed to avoid uneven aging or deactivation of the catalyst [2]. The flow distribution in the radial-flow process can be studied using a computational fluid dynamics (CFD) model to understand the complicated changes of flow direction in the system.

Radial flow reactors differ from more commonly used axial flow reactors. In an axial flow reactor, feed enters at one end of a tube packed with catalyst particles, flows through the catalyst bed in the direction along the axis of the reactor, and exits from the other end. In comparison, a radial flow reactor is designed so that the feed is distributed along the length of the catalyst bed and flows radially through the bed (see Figure 1). The distance that the feed travels through the catalyst bed is shorter, thus reducing pressure drop in large volume processes.

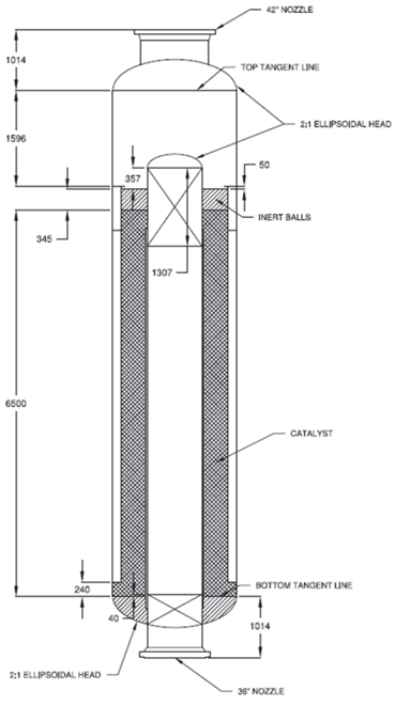

Figure 1. Schematic of radial-flow fixed bed.

The design of the radial flow reactor is more complicated than that of the axial flow reactor [1, 3]. There are some concerns that are unique to designing the radial flow reactor:

- The flow can enter and exit the reactor at the same end (π-configuration) or at opposite ends (Z-configuration). The flow can be

directed radially outward (CF-flow) or inward (CP-flow). In this study only Z-configuration is studied, with CP-flow (normal flow) and CF-flow (reverse flow).

- Over time, catalyst settling will create a void space at the top of a radial catalyst bed, which could allow flow bypassing. Extra catalyst is normally loaded to allow for settling resulting in an axial-flow region [4].
- A radial flow reactor requires an inlet distributor to provide flow along the length of the reactor [1], as well as a collector to provide for the exiting flow.

The system efficiency and its cost-effectiveness are strongly influenced by the screen design [5]. Screens are used to contain the catalyst bed and also control the amount of flow that goes through the bed. They should be designed to withstand the thermal stresses that develop with each startup and shutdown process of the reactor [1].

2. Model Equations

The model equations are given here in dimensional form. Turbulent incompressible flow was used for all regions of the reactor, with terms added to represent forces acting on the fluid per unit volume in the catalyst bed and screen regions of the domain [6].

Values of the constants and bed properties under base case conditions are given in Table 1 in the Appendix. Baseline conditions were for 10% open screens and cylindrical pellets with D = ⅛ in. and L = 3/16 in. so that d_p was the diameter of the equivalent volume sphere..

2.1 Mass and momentum balances

The equations for the mass and momentum balances are:

$$\rho(\mathbf{u}\cdot\nabla)\mathbf{u} = \nabla\cdot\left[-\rho\mathbf{I} + (\mu+\mu_T)(\nabla\mathbf{u} + (\nabla\mathbf{u})^T) - \frac{2}{3}\rho k I\right] + \mathbf{F} \quad (1)$$

$$\rho\nabla\cdot\mathbf{u} = 0 \quad (2)$$

The term **F** represents forces acting on the fluid per unit volume. Turbulence was modeled by the *k*-ε RANS approach, with the equations:

$$\rho(\boldsymbol{u}\cdot\nabla)k = \nabla\cdot\left[\left(\mu+\frac{\mu_T}{\sigma_k}\right)\nabla k\right] + P_k - \rho\varepsilon \quad (3)$$

$$\rho(\boldsymbol{u}\cdot\nabla)\varepsilon = \nabla\cdot\left[\left(\mu+\frac{\mu_T}{\sigma_e}\right)\nabla\varepsilon\right] + C_{e1}\frac{\varepsilon}{k}P_k - C_{e2}\rho\frac{\varepsilon^2}{k} \quad (4)$$

$$\mu_T = \rho C_\mu \frac{k^2}{\varepsilon} \quad (5)$$

$$P_k = \mu_T[\nabla\mathbf{u}:(\nabla\boldsymbol{u} + (\nabla\boldsymbol{u})^T)] \quad (6)$$

The turbulence model parameters were

$$C_{e1} = 1.44 \quad C_{e2} = 1.92 \quad C_\mu = 0.09$$
$$\sigma_k = 1 \quad \sigma_e = 1.3$$

2.2 Catalyst bed

The equation for **F** in the catalyst bed was:

$$\mathbf{F} = -\frac{\mu}{K} * \boldsymbol{u} - \frac{C_{2B} * \rho}{2}|\boldsymbol{u}|\boldsymbol{u} \quad (7)$$

This is the Darcy-Forchheimer Law which describes single-phase laminar flow through a porous medium, including a term to describe the inertial resistance. Values for *K* and *C2B* in the bed were obtained from the Ergun equation for pressure drop in a packed bed, which depends on the particle size and bed void fraction:

$$\mathrm{K} = \frac{d_p^2\epsilon^3}{150(1-\epsilon)^2} \quad C_{2B} = \frac{3.5(1-\epsilon)}{d_p\epsilon^3} \quad (8)$$

2.3 Screen regions

The resistance in the screens was given by the porous jump model [2] as:

$$\mathbf{F} = -\frac{C_{2S}*\rho}{2}|\boldsymbol{u}|\boldsymbol{u} \quad (9)$$

Different values for the inertial resistance C_{2S} could be used for the inner and outer screens. Values for C_{2S} were determined from the equation of flow through square-edged holes on an equilateral triangular spacing [2].

$$\boldsymbol{C_{2S}} = \frac{\left(\frac{A_p}{A_f}\right)^2 - 1}{C^2\Delta x} \quad (10)$$

where A_p is the screen area, A_f is the free (open) screen area, Δx is screen thickness and C is the orifice coefficient for the holes. The flow resistance could be adjusted by changing the open area fraction of the screens and/or the catalyst particle diameter in the bed.

2.4 Maldistribution

The maldistribution index is a measure of axial non-uniformity in the radial flow through the catalyst bed [7]. In this work, the average radial velocity at a given radius was used as a measure of a uniform flow. The maldistribution index was then defined as

$$\mathrm{M}(r) = \frac{1}{L}\int_0^L \sqrt{\left(u_r - u_{r,av}\right)^2}\,dz \qquad (11)$$

where L is the catalyst bed length.

3. Use of COMSOL Multiphysics®

Our approach used the 2D axisymmetric modeling capabilities of COMSOL Multiphysics® to draw the complex reactor geometry. The model domain contained both large and very small regions, shown in Figure 2.

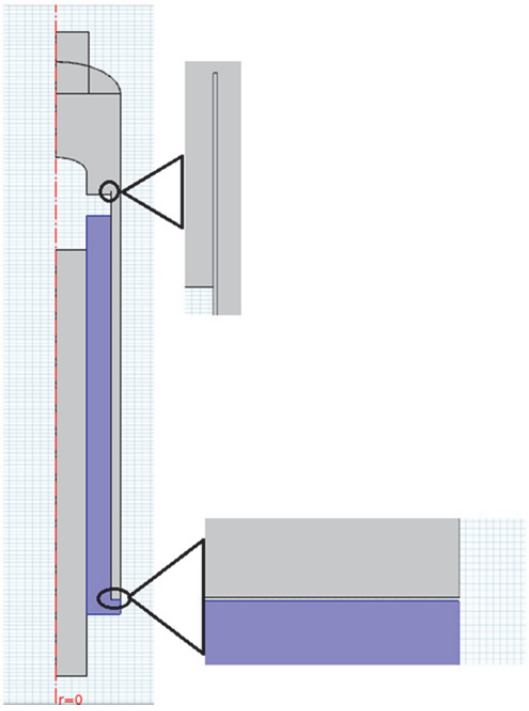

Figure 2. Model geometry, showing thin screen regions and spacing between channels and bed.

The model equations were solved using the finite element method as implemented in COMSOL Multiphysics®. The CFD Module was selected as it enabled single phase turbulent flow modeling, using the Reynolds-Averaged Navier-Stokes (RANS) approach. In addition, user-defined volume force terms were available.

The computational domain was meshed using the physics-controlled mesh capability of COMSOL Multiphysics® with the extremely coarse setting, resulting in 551935 degrees of freedom. Part of the mesh is shown in Figure 3:

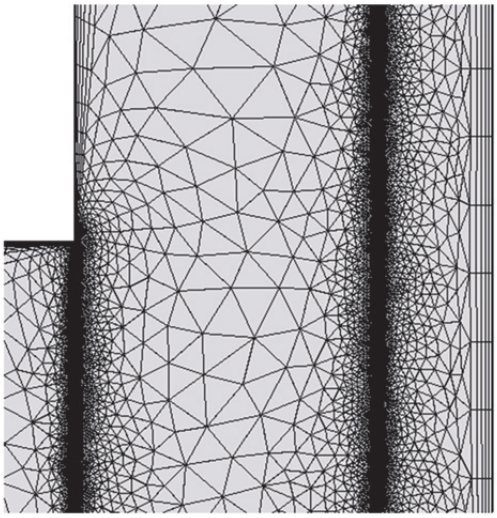

Figure 3. Unstructured mesh showing details of the refined mesh in and close to the screen regions and structured mesh adjacent to no-slip boundaries.

A refined mesh of 728355 degrees of freedom under the extra coarse setting was also run for both normal and reverse flows and results for pressure and velocity differed by less than 0.5% showing mesh independence.

Boundary conditions were set as a given inlet velocity and outlet pressure. Convergence was not easy to obtain, and it was necessary to use auxiliary parametric continuation. The volume force terms in the bed and screens were initially set to zero, the model converged and then the forces were increased to their correct values in a series of incremental steps, converging the model at each step. Typical computation times on a server running dual processors at 3.50 GHz with 128 GB under a 64-bit Windows operating system were between 46 and 86 minutes.

4. Results and Discussion

The results are presented first in terms of flow and pressure contours for the base case, to illustrate the complex flow patterns inside the reactor. The effects of changing bed and screen resistances are discussed next, followed by the comparison between normal and reverse flow.

4.1 Base case flow simulations

An overall understanding of the normal flow inside the reactor can be obtained from Figure 4. Flow enters at the top, and is then accelerated as it is forced into the narrow outer shell. Radial velocities across the catalyst bed are much lower, while the axial velocity in the inner annulus increases from zero to a quite high value. The high velocity region near the exit is caused by the constriction of the axial flow due to radial flow from the bed.

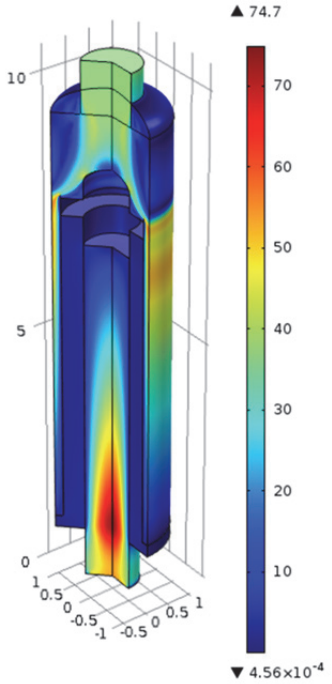

Figure 4. 3D view of internal flows in the reactor.

Pressure contours on a cross-section of the reactor are shown in Figure 5. The fluid in the normal flow model experiences significant pressure drop before the catalyst bed. In the bed, pressure drop is higher at the top of the bed outlet, leading to maldistribution in the radial flow. For reverse flow, most of the pressure drop was experienced inside the catalyst bed.

Figure 6 indicates that the normal flow had considerable fluid recirculation, in the top right region of the reactor, as well as in a small pocket (inset) at the top of the outer annulus and the top right of the catalyst bed. The reverse flow streamlines, in contrast, did not show significant recirculation, although there must be a stagnant region as the flow exits from the outer annulus.

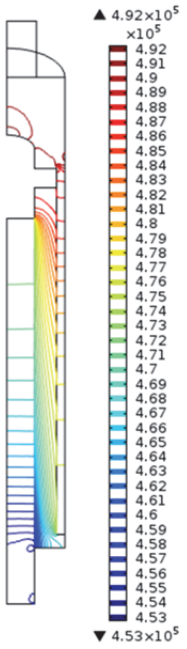

Figure 5. Pressure contour plot for normal flow. Red represents high pressure, blue represents low.

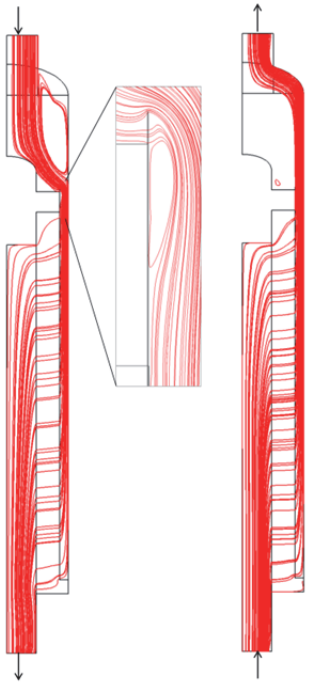

Figure 6. Velocity streamline plots, for normal flow (left) and reverse flow (right).

Figure 7 shows the flow field and re-circulation regions for normal flow that are associated with higher resistance to flow, which suggests where re-design of the reactor could be beneficial to reduce pressure drop.

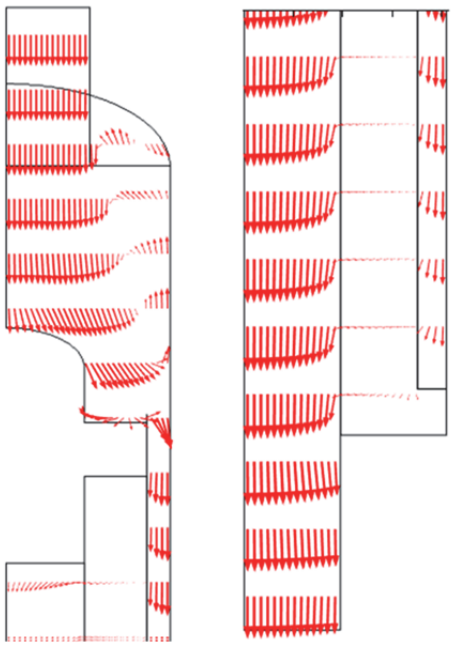

Figure 7. Velocity vector plots for normal flow, focusing on the top and bottom of the catalyst bed.

4.2 Effects of bed and screen resistances

Figure 8 shows the changes in catalyst bed pressure drop due to bed and screen resistance.

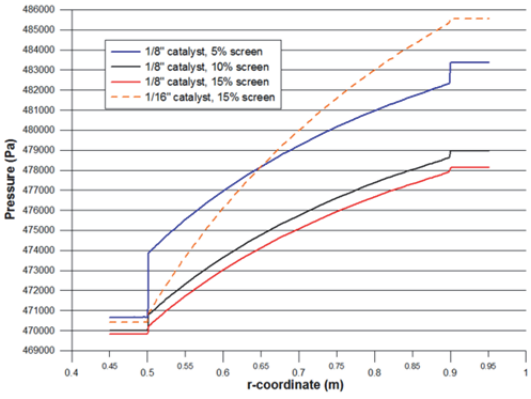

Figure 8. Comparison of radial pressure profiles across bed and screens, for different screen open fractions and bed particle size.

Three values for screen open area fraction were compared, and two sizes of catalyst particle. Higher open area and larger pellets reduce ΔP but also increase by-passing flow in the bed, giving catalyst underutilization and/or non-uniform deactivation. The screen flow resistance is small for open area fractions above 10%.

Figure 9 shows the corresponding radial velocity profiles along the bed axial coordinate, for the same three screen openings and catalyst particle sizes. There is a variation in radial velocity along the bed length, with the decrease at low z being attributable to the region of mixed flow in the packing at the top of the bed, while the strong decrease at large z is caused by the approach to zero flow in the outer annulus feeding the bed. The average bed velocity increases almost linearly with screen open fraction, as total resistance to flow is decreased. The screen resistance does not have a strong impact on the velocity distribution in the middle of the bed, although there is some effect near the inlet. The value of M increases from 0.156 to 0.178 as screen opening goes from 5% to 15%. The smaller catalyst particles give a larger pressure drop in the bed, but also provide a more uniform distribution of velocity, as M decreases to 0.149 on going to the smaller catalyst size..

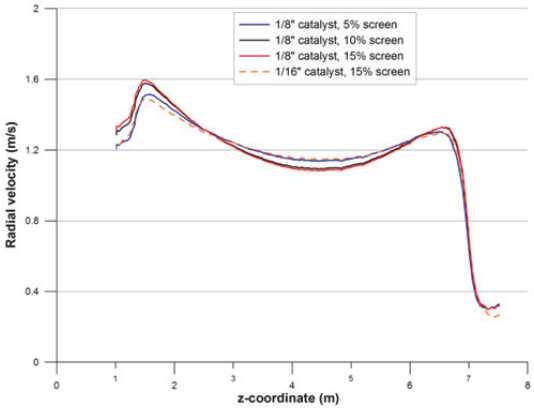

Figure 9. Axial profiles along bed length of radial velocity component, for different screen open fractions and bed particle size.

4.3 Effect of flow direction

The impact of changing the flow direction is illustrated in Figure 10, showing the two radial

velocity profiles obtained. Both profiles show that there is lower flow in the bed close to the top and bottom walls of the bed. The reverse flow has a less uniform radial velocity distribution than the normal flow. For normal flow, the maldistribution index M = 0.17, while for reverse flow it is M = 0.43.

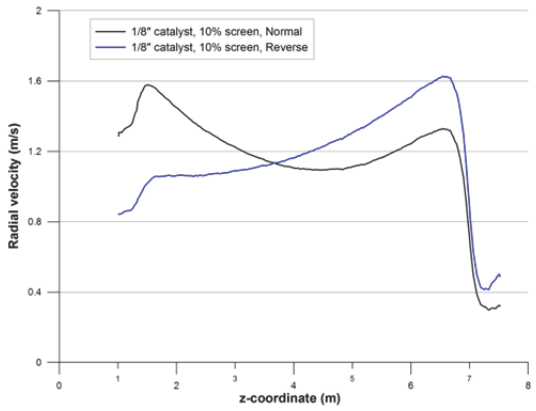

Figure 10. Axial profile of radial velocity distribution, for normal (inwards) and reverse (outwards) flow cases.

5. Conclusions

Resistance to flow can be decreased by larger catalyst particles or more open screens, but this may lead to more severe flow maldistribution. Normal flow was found to give better flow distribution in this configuration than reverse flow.

6. References

1. Li, J. C. H., Radial-flow packed-bed reactors, in Ullmann's Encyclopedia of Industrial Chemistry, Wiley-VCH Verlag GmbH & Co., Weinheim (2012).
2. Kareeri, A. A., Zughbi, H. D., and Al-Ali, H. H., Simulation of flow distribution in radial flow reactors, *Ind. Eng. Chem. Res.,* **45**, 2862-2874 (2006).
3. Chang, H., & Calo, J. M., An analysis of radial flow packed bed reactors: How are they different? *ACS Symposium Series,* **168**, 305-329 (1981).
4. Yoo, C-S., and Dixon, A. G., Modelling and simulation of a mixed-flow reactor for ammonia and methanol synthesis. *Chem. Eng. Sci.,* **43**, 2859-2865 (1988).
5. Johnson Screens. (2010). *Internals for radial flow reactors.* Retrieved 12/14, 2014, from http://www.johnsonscreens.com/sites/default/files/6/705/Internals%20for%20Radial%20Flow%20Reactors.pdf
6. Ranade, V. V. *Computational flow modeling for chemical reaction engineering,* Ch. *5* (pp. 403-423). San Diego, CA: Academic Press (2002).
7. Yoo, C.-S. and Dixon, A.G., Maldistribution in the radial-flow fixed bed reactor, pp 749-757 in H.I. de Lasa (ed.) "Chemical Reactor Design and Technology", NATO ASI Series E - No. 110 (1986).

7. Acknowledgements

We would like to thank Waheed Mukaddam and Enrique Cintron of CCTI (Cambridge Chemical Technologies, Inc.) for their support of our project and for their help and technical advice.

8. Appendix

Table 1: Constants used in base case model

Quantity (f: feed)	Value	Description
μ	1.94×10^{-5} kg/m·s	Fluid viscosity
ρ_f	2.42 kg/m^3	Fluid density
d_p	0.0042 m	Catalyst particle diameter
ϵ	0.36	Catalyst bed void fraction
A_{p0}	37.6 m^2	Outlet screen area
C	0.62	Orifice coefficient
Δx	0.001	Screen thickness
A_{pi}	18.52 m^2	Inlet screen area